Li, Diao; Xue, Hui; Wang, Yadong; Qi, Mei; Kim, Wonjae; Li, Changfeng; Riikonen, Juha; Ren, Zhaoyu; Bai, Jintao; Lipsanen, Harri; Sun, Zhipei

Active synchronization and modulation of fiber lasers with a graphene electro-optic modulator

Published in:
Optics Letters

DOI:
10.1364/OL.43.003497

Published: 01/08/2018

Document Version
Publisher's PDF, also known as Version of record

Please cite the original version:
Li, D., Xue, H., Wang, Y., Qi, M., Kim, W., Li, C., Riikonen, J., Ren, Z., Bai, J., Lipsanen, H., & Sun, Z. (2018). Active synchronization and modulation of fiber lasers with a graphene electro-optic modulator. *Optics Letters*, *43*(15), 3497-3500. https://doi.org/10.1364/OL.43.003497

Optics Letters

Active synchronization and modulation of fiber lasers with a graphene electro-optic modulator

Diao Li,[1,2] Hui Xue,[2] Yadong Wang,[2,3] Mei Qi,[1,2] Wonjae Kim,[2,4] Changfeng Li,[2] Juha Riikonen,[2] Zhaoyu Ren,[1] Jintao Bai,[1,*] Harri Lipsanen,[2] and Zhipei Sun[2,5,6]

[1]State Key Lab Incubation Base of Photoelectric Technology and Functional Materials, and Institute of Photonics and Photon-Technology, Northwest University, 710069 Xi'an, China
[2]Department of Electronics and Nanoengineering, Aalto University, Tietotie 3, FI-02150 Espoo, Finland
[3]MOE Key Laboratory of Material Physics and Chemistry under Extraordinary Conditions, and Shaanxi Key Laboratory of Optical Information Technology, School of Science, Northwestern Polytechnical University, Xi'an 710072, China
[4]VTT Technical Research Center of Finland, Tietotie 3, 02150 Espoo, Finland
[5]QTF Centre of Excellence, Department of Applied Physics, Aalto University, FI-00076 Aalto, Finland
[6]e-mail: zhipei.sun@aalto.fi
*Corresponding author: baijt@nwu.edu.cn

Received 27 April 2018; revised 18 June 2018; accepted 20 June 2018; posted 21 June 2018 (Doc. ID 329017); published 17 July 2018

We report the synchronization of two actively *Q*-switched fiber lasers operating at 1.5 μm and 2 μm with a shared broadband graphene electro-optic modulator. Two graphene monolayer sheets separated with a high-*k* HfO_2 dielectric layer are configured to enable broadband light modulation. The graphene electro-optic modulator is shared by two optical fiber laser cavities (i.e., an erbium-doped fiber laser cavity and a thulium/holmium-codoped fiber laser cavity) to actively *Q*-switch the two lasers, resulting in stable synchronized pulses at 1.5 μm and 2 μm with a repetition rate ranging from 46 kHz to 56 kHz.

OCIS codes: (160.4236) Nanomaterials; (230.4110) Modulators; (230.2090) Electro-optical devices; (140.3540) Lasers, Q-switched; (140.3538) Lasers, pulsed.

https://doi.org/10.1364/OL.43.003497

Synchronized optical pulses at different wavelengths have attracted increasing research interest due to their great potential in applications such as Raman scattering spectroscopy [1] and nonlinear frequency conversion [2]. Pulse synchronization is typically classified to passive and active approaches. In the passive approach, a saturable absorber (SA) with broad operation bandwidth covering multiple laser wavelengths is used to enable self-modulation by positioning it in a common arm of the cavities [3–8]. For the active approach, an externally controlled optical modulator (e.g., electro-optic modulator) with wide operation bandwidth is needed. To achieve synchronized pulsed lasers, *Q*-switching and mode-locking technologies are commonly used [3–8]. Reference [5] introduced a passively synchronized mode-locking in erbium-doped fiber (EDF) and thulium-doped fiber lasers by incorporating a graphene SA in a common branch of two fiber ring cavities. Both laser loops were passively synchronized at 20.5025 MHz by nonlinear interaction between generated pulses. Despite that graphene has been extensively demonstrated as a broadband SA for multi-wavelength mode-locking [9–11], a precisely mechanical alignment is indispensable to match the fiber cavity length and to start the synchronization operation [5]. References [4,6] reported the formation of graphene SA *Q*-switched laser synchronization in solid-state and fiber cavities. It should be noted that the cavity length is not required to be strictly identical for pulse synchronization in *Q*-switching, as the pulse repetition rates are strongly dependent on the *Q*-factor dynamics. Therefore, pump power can be a dominant parameter for starting and breaking the *Q*-switching synchronization in these lasers [8]. In comparison with passively modulated lasers [4–8], synchronized lasers mode-locked or *Q*-switched with active modulators were barely explored. One of the possible reasons is lack of active devices having a broad operation bandwidth. For example, the operation bandwidth of conventionally used bulk electro-optic modulators is typically limited (e.g., ∼100 nm at the infrared spectral region [12]), which cannot cover the relatively large bandwidth between two typical technological wavelengths [e.g., >400 nm (between 1.5 and 2 μm)]. Therefore, developing novel active optical modulators with broadband response becomes a key solution to overcome the shortcomings of traditional bulk materials-based modulators.

Recently, graphene [13] and other two dimensional layered materials (e.g., MoS_2 [14–16], black phosphorus [17–20]) have greatly attracted the research attention in active optoelectronic devices owing to their unique physical properties. One of the rapidly developed optoelectronic devices is graphene electro-optic modulators (GEOMs) [12,21], which have been demonstrated as a promising alternative to traditional bulk materials-based modulators due to their superior performance, such as broadband and ultrafast response, miniature footprint, and low power consumption [21]. These suggest GEOM an ideal platform for optical pulse generation in lasers through active modulation. In fact, a group of successful paradigms have been identified by using graphene modulators as electrically controlled SAs [22–25] (i.e., active and passive hybrid laser modulation). However, it is challenging to directly generate active synchronization within these lasers because the saturable absorption effect plays dominant roles in the pulse formation process. Very recently, pulsed fiber lasers actively Q-switched and mode-locked by GEOMs were demonstrated [12,26].

In this Letter, for the first time to the best of our knowledge, we demonstrate actively synchronized Q-switching of two fiber lasers (at 1.5 μm and 2 μm) with a GEOM. The GEOM is configured with two monolayer graphene sheets isolated by a hafnium dioxide (HfO_2) dielectric layer. Synchronized Q-switching is observed in two fiber laser cavities [i.e., EDF and thulium/holmium-codoped fiber (THDF) lasers] through inserting the GEOM in the common branch of the two fiber cavities. The two lasers can be converted from continuous wave (CW) to Q-switching operation simultaneously with synchronized oscillation. The synchronized Q-switching repetition rate ranges from 46 kHz to 56 kHz. Pulses with energy up to 130.2 nJ (86.7 nJ) and pulse duration down to 7.4 μs (9.6 μs) are obtained at 1561.3 nm (1900.8 nm) when the repetition rate is 46 kHz. In contrast with passively Q-switched operation where the pump power needs to be precisely controlled to start and maintain the synchronization, our graphene-based active modulation approach provides a simpler option to achieve broadband pulse synchronization.

A simplified schematic image of the GEOM is shown in Fig. 1(a). Two monolayer graphene sheets are parallelly aligned to form a capacitor configuration, which is isolated by a high-k HfO_2 dielectric layer as follows: the graphene capacitor is supported by a quartz plate. Monolayer graphene prepared with chemical vapor deposition approach is wet transferred onto the quartz substrate. After, an evaporation-deposited titanium and gold contact (5 nm and 50 nm) is patterned by electron beam lithography (EBL, Vistex EPBG5000pES). To reduce the RC time constant, the large graphene sheet is patterned to a miniature footprint (500 μm × 500 μm) with EBL and reactive ion etching. A high permittivity HfO_2 layer (30 nm thick) is then grown on the entire device to form an insulating separation. The HfO_2 is deposited by pulsing Tetrakis (dimethylamido) hafnium (TDMAH ≡ $HfN_4C_8H_{24}$) and water in an alternating fashion with atomic layer deposition (ALD) [27]. Prior to pulsing, the solid TDMAH-precursor is sublimated by heating it at 50°C. The ALD process is carried out at 170°C to ensure the high quality of the HfO_2 film. After the deposition, the growth rate (∼0.991 Å/cycle) of the HfO_2 film is measured from a reference silicon substrate by using a commercial ellipsometer. The graphene capacitor configuration is formed after transferring a new monolayer graphene layer on the top. The GEOM is formed after the top graphene and metal electrodes are patterned and evaporated by using the same procedures of their bottom counterparts. Raman spectra of the bottom graphene layer before and after the HfO_2 film deposition are shown in Fig. 1(b). No obvious defect feature (D peak) arises in the Raman spectrum after the HfO_2 layer deposition, demonstrating that there is no obvious damage in graphene during ALD film deposition. Figure 1(c) depicts the measured voltage-dependent optical transmittance at 1550 nm. The GEOM presents a modulation depth of ∼0.7% with the applied voltage range from 0 V to 3.1 V. The inset of Fig. 1(c) shows a calculated Fermi level shift as a function of voltage, giving a 0.23 eV variation in the corresponding applied voltage range. Voltage-dependent optical transmittance at 2 μm is not obtainable because of the lack of a highly stable light source (with power fluctuation <0.1%) in our laboratory. The dynamic electro-optical response of the GEOM is investigated using a radio frequency (RF) lock-in amplifier connected with a 22 GHz photodiode. The results [Fig. 1(d)] give a 3 dB bandwidth ($f_{3\,\mathrm{dB}}$) of ∼600 kHz.

Figure 2 illustrates the schematic of our actively synchronized Q-switched fiber laser. The broadband GEOM is used as an active Q-switch, which is placed in a common branch of two fiber cavities configured at 1.5 μm and 2 μm, respectively. A 1550/2000 nm wavelength division multiplexer (WDM) is selected to combine and split the light from the 1.5 μm and 2 μm cavities in and out from the common branch. Lenses L1 and L2 are fixed close to the common fiber end to assure effective beam coupling between optical fiber and the GEOM. The GEOM serves as an active switch to actively modulate the Q-factor of both laser cavities by externally applied signal. A gold-coated mirror with high reflection (>99% in a wavelength range between 1500 nm and 2000 nm) is positioned at the focal point to feedback the light

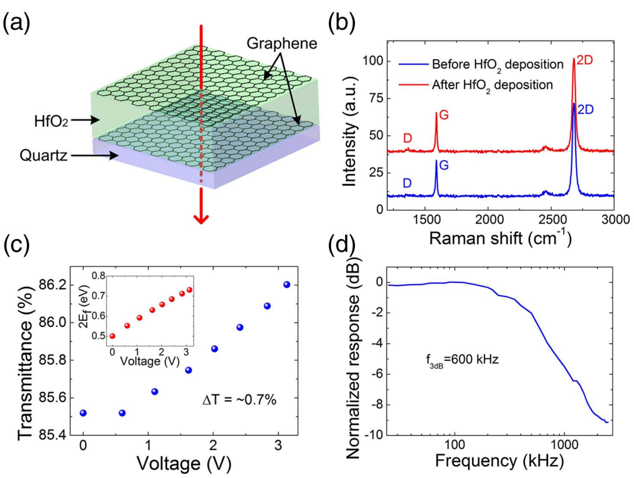

Fig. 1. (a) Schematic of the GEOM. (b) Raman spectra of the bottom graphene layer. (c) Transmittance of the GEOM as a function of signal voltage. Inset, calculated Fermi level shift as a function of voltage. (d) Dynamic response.

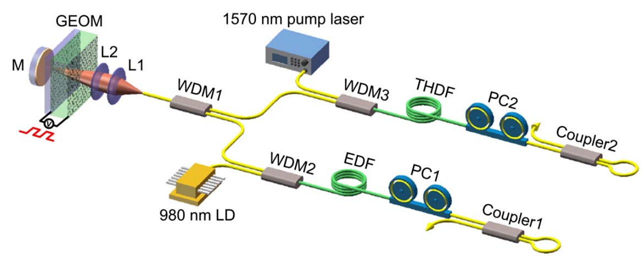

Fig. 2. Schematic setup of actively synchronized Q-switched fiber lasers. L1, collimating lens; L2, focusing lens; M, reflection mirror; WDM1, 1550/2000 nm wavelength division multiplexer; LD, laser diode; WDM2, 980/1550 nm wavelength division multiplexer; WDM3, 1570/2000 nm wavelength division multiplexer; EDF, erbium-doped fiber; THDF, thulium/holmium-codoped fiber; PC1 and PC2, polarization controller; Coupler1 and Coupler2, output coupler.

to fiber components. A 980/1550 nm WDM (WDM2 in Fig. 2) is connected to the 1550 nm port of WDM1. A segment of 1 m EDF is used as the gain medium at 1550 nm. A 980 nm laser diode is employed to pump the EDF through WDM2. After the EDF, a fiber in-line polarization controller is connected to adjust the birefringence of the cavity. A 90/10 coupler is used to provide reflection and output of the intracavity light with a closed loop. The 10% port is employed for output. In the 2 μm laser cavity, a section of 2 m THDF is used to provide gain for the laser, which is pumped with a 1570 nm homemade amplified fiber laser through a 1570/2000 nm WDM (WDM3 in Fig. 2). A PC and a 90/10 coupler at 2 μm are used to adjust the polarization state and output the intracavity light (via 10% port). The lengths of the two individual cavities are 7.3 m and 8.5 m (including the common branch of 1.3 m), respectively. An electric signal generator is employed to provide frequency and amplitude adjustable square wave signal to the GEOM device. The performance of the synchronously Q-switched lasers is characterized with a high-resolution optical spectrum analyzer (Anritsu, MS9740A), a frequency spectrum analyzer (Anritsu, MS2692A), a power meter (Ophir, Nova II), a broadband ultrafast photodetector, and a digital oscilloscope.

Oscillation status of the laser cavities is strongly dependent on a few parameters including pump power, signal voltage, and modulation frequency in the case that the GEOM device is used. Three laser regimes including CW, independent Q-switching, and synchronized Q-switching oscillations can be obtained according to the adjustment of the signal voltage and the pump power. In the first case, i.e., when the electric signal is not applied on the GEOM, only CW lasers at 1.5 μm and 2 μm are observed, which indicates that the graphene layers are not able to be saturated by the intracavity light (i.e., passive Q-switching operation cannot self-start). Figure 3 depicts the CW laser output power as a function of the pump power (red dots). Power conversion efficiencies are calculated as 13.75% and 3.5% for 1.5 μm and 2 μm, respectively.

When a square wave signal is applied on the GEOM device, active Q-switching can be initiated by tuning the modulation frequency. Both CW lasers can be turned from CW operation into the Q-switching state independently. It is noteworthy that the minimum and maximum output repetition rates (i.e., repetition rate range) of each Q-switched laser exhibit a strong power dependence. To quantify this, we investigate the relation between the minimum Q-switching repetition rate and the pump power. As shown in Fig. 3 (blue squares), the minimum repetition rate increases from 14 kHz (25 kHz) to 63 kHz (74 kHz) at different pump powers ranging from 12.7 mW (339 mW) to 87.1 mW (472 mW) at 1.5 μm (2 μm). It is then feasible to acquire Q-switched pulse synchronization between the two lasers via controlling the pump powers and the modulation frequency precisely. After a synchronized operation is started, the repetition rates of the two laser pulse trains are equivalent to the electric modulation frequency and can be simultaneously adjusted.

As a typical example, the two lasers synchronously Q-switch at a repetition rate of 46 kHz when the pump powers are set at 50.9 mW and 393 mW for 1.5 μm and 2 μm, respectively. Upon further increase of the modulation frequency, the pulse synchronization can sustain to a higher repetition rate of 56 kHz. Figure 4(a) presents a square wave signal and the synchronized Q-switching pulse trains corresponding to the minimum repetition rate of 46 kHz at ~1.5 μm and 2 μm, respectively, which gives the pulse durations of 7.4 μs and 9.6 μs. Figure 4(b) represents the measured output laser spectra of the synchronously Q-switched lasers. The lasers center at 1561.3 nm and 1900.8 nm, showing a full width at half-maximum of 0.5 nm and 1.5 nm, respectively.

The pulsed lasers exhibit a typical active Q-switching character. The output pulse energy and duration are both pump power dependent when the external modulation frequency is fixed. Figures 5(a) and 5(b) show that the pulse duration

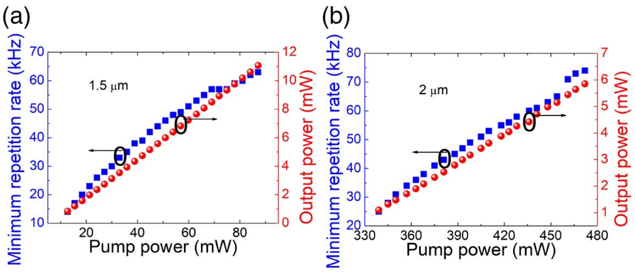

Fig. 3. CW laser output power (red dots) and minimum Q-switching repetition rate (blue squares) as a function of the pump power at (a) ~1.5 μm and (b) 2 μm.

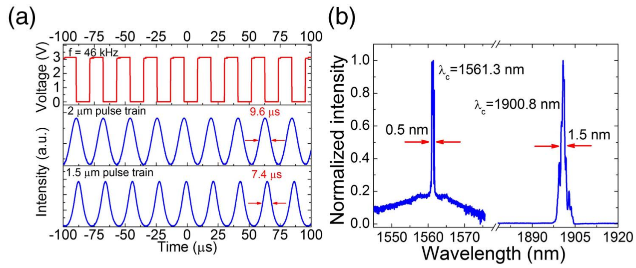

Fig. 4. (a) Electric signal (top panel) and synchronously Q-switched pulse trains (middle panel for 2 μm and bottom panel for 1.5 μm lasers). (b) Synchronously Q-switched laser output spectra at ~1.5 μm (left panel) and 2 μm (right panel).

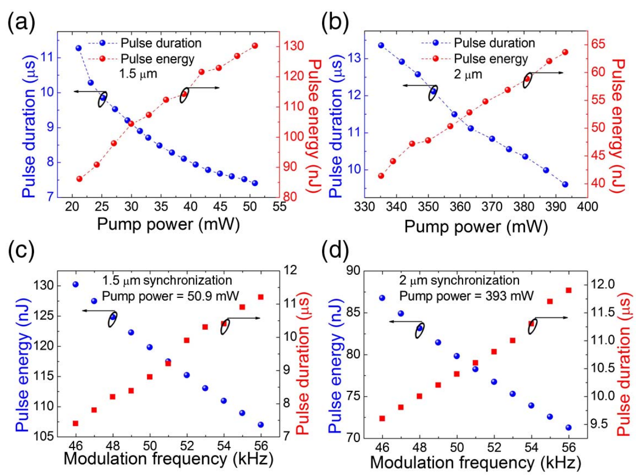

Fig. 5. Output pulse duration and energy as a function of the pump power at (a) 1.5 μm and (b) 2 μm when the modulation frequency is fixed at 46 kHz. Output pulse energy and duration of the synchronized lasers as a function of the modulation frequency at (c) ~1.5 μm and (d) 2 μm.

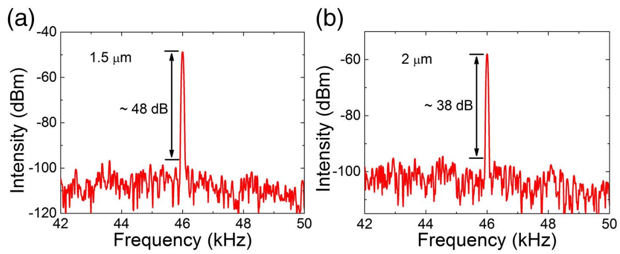

Fig. 6. Radio frequency spectra of the Q-switched lasers of (a) 1.5 μm and (b) 2 μm at 46 kHz repetition rate.

decreases from 11.3 μs (13.4 μs) to 7.4 μs (9.6 μs) at 1.5 μm (2 μm) when the pump power is increased from 21.1 mW (335.3 mW) to 50.9 mW (393 mW). Meanwhile, the pulse energy increases from 86.1 nJ (41.4 nJ) to 130.2 nJ (63.6 nJ). In addition, the pulse duration and pulse energy of our actively Q-switched lasers are also frequency dependent. As shown in Figs. 5(c) and 5(d), at the fixed pump power of 50.9 mW (393 mW) and modulation voltage of 3.1 V, Q-switched pulse duration increases from 7.4 μs (9.6 μs) to 11.2 μs (11.9 μs), and pulse energy reduces from 130.2 nJ (86.7 nJ) to 107 nJ (71.2 nJ) for the 1561.3 nm (1900.8 nm) laser when the modulation frequency is increased from 46 kHz to 56 kHz. This can be interpreted by the time-dependent dynamic evolution relation between the gain and loss in Q-switched lasers: as the modulation frequency increases, the energy stored in the gain fiber per switching cycle reduces and therefore releases longer pulse with lower pulse energy. This allows to adjust the output parameters of the synchronized pulses more flexibly in addition to the power-dependent adjustment approach. In order to evaluate the Q-switching stability, we measure the RF spectra of each laser around the minimum pulse repetition rate of 46 kHz. As shown in Fig. 6, the signal-to-noise ratios are 48 dB ($\sim 10^5$ contrast) and 38 dB ($\sim 10^4$ contrast) corresponding to ~1.5 and 2 μm, respectively, which confirm good pulse stability for both lasers. The relatively lower contrast (i.e., stronger noise) of the 2 μm laser is mainly caused by the lower power fluctuations (~3%) of its pump source.

In conclusion, we demonstrate synchronized Q-switched fiber lasers with a GEOM. A capacitive modulator configured with two monolayer graphene sheets is used to actively modulate the Q-factors of two laser cavities, respectively. In a typical synchronization operation, Q-switched laser repetition rate variation between 46 kHz and 56 kHz is observed when the pump powers are fixed to 50.9 mW and 393 mW corresponding to the laser wavelengths of 1561.3 nm and 1900.8 nm, respectively. Particularly, the pulse duration increases from 7.4 μs (9.6 μs) to 11.2 μs (11.9 μs), and the pulse energy reduces from 130.2 nJ (86.7 nJ) to 107 nJ (71.2 nJ) for the 1561.3 nm (1900.8 nm) laser. Our results identify graphene a promising electro-optic material for actively modulated pulse generation over a broadband wavelength range via means of active modulation rather than passive absorption modulation.

Funding. European Union's Seventh Framework Programme (631610, 696656); Academy of Finland (276376, 284548, 295777, 304666, 312297, 312551, 314810); China Scholarship Council (CSC); International Science and Technology Cooperation Project (2014DFR10780); National Science Foundation for Young Scholars of China (61505162); Natural Science Basic Research Plan in Shaanxi Province of China (2016JQ6059); Foundation of the Education Committee of Shaanxi Province (14JK1756).

Acknowledgment. The authors acknowledge the provision of technical facilities of the Micronova, Nanofabrication Centre of Aalto University. Y. W. thanks Jakub Boguslawski for his help on dynamic measurement.

REFERENCES

1. E. O. Potma, D. J. Jones, J. X. Cheng, X. S. Xie, and J. Ye, Opt. Lett. **27**, 1168 (2002).
2. E. Herault, M. Lelek, F. Balembois, and P. Georges, Opt. Express **16**, 19419 (2008).
3. M. Zhang, E. J. R. Kelleher, A. S. Pozharov, E. D. Obraztsova, S. V. Popov, and J. R. Taylor, Opt. Lett. **36**, 3984 (2011).
4. P. Tidemand-Lichtenberg, J. Janousek, R. Melich, J. L. Mortensen, and P. Buchhave, Opt. Commun. **241**, 487 (2004).
5. J. Sotor, G. Sobon, J. Tarka, T. Pasternak, A. Krajewska, W. Strupinski, and K. M. Abramski, Opt. Express **22**, 5536 (2014).
6. J. Janousek, P. Tidemand-Lichtenberg, J. L. Mortensen, and P. Buchhave, Opt. Commun. **265**, 277 (2006).
7. H. P. H. Cheng, P. Tidemand-Lichtenberg, O. B. Jensen, P. E. Andersen, P. M. Petersen, and C. Pedersen, Opt. Express **18**, 23987 (2010).
8. D. Wu, Z. Luo, F. Xiong, C. Zhang, Y. Huang, S. Chen, W. Cai, Z. Cai, and H. Xu, IEEE Photon. Technol. Lett. **26**, 1474 (2014).
9. J. Sotor, G. Sobon, I. Pasternak, A. Krajewska, W. Strupinski, and K. M. Abramski, Opt. Express **21**, 18994 (2013).
10. B. Fu, Y. Hua, X. Xiao, H. Zhu, Z. Sun, and C. Yang, IEEE J. Sel. Top. Quantum Electron. **20**, 1100705 (2014).
11. Z. Sun, D. Popa, T. Hasan, F. Torrisi, F. Wang, E. J. R. Kelleher, J. C. Travers, V. Nicolosi, and A. C. Ferrari, Nano Res. **3**, 653 (2010).
12. D. Li, H. Xue, M. Qi, Y. Wang, S. Aksimsek, N. Chekurov, W. Kim, C. Li, J. Riikonen, F. Ye, Q. Dai, Z. Ren, J. Bai, T. Hasan, H. Lipsanen, and Z. Sun, 2D Mater. **4**, 025095 (2017).
13. F. Bonaccorso, Z. Sun, T. Hasan, and A. C. Ferrari, Nat. Photonics **4**, 611 (2010).
14. A. Säynätjoki, L. Karvonen, H. Rostami, S. Mehravar, A. Lombardo, R. A. Norwood, T. Hasan, N. Peyghambarian, H. Lipsanen, K. Kieu, A. C. Ferrari, M. Polini, and Z. Sun, Nat. Commun. **8**, 893 (2017).
15. H. Chen, J. Yin, J. Yang, X. Zhang, M. Liu, Z. Jiang, J. Wang, Z. Sun, T. Guo, W. Liu, and P. Yan, Opt. Lett. **42**, 4279 (2017).
16. F. Bonaccorso and Z. Sun, Opt. Mater. Express **4**, 63 (2014).
17. A. Autere, H. Jussila, Y. Dai, Y. Wang, H. Lipsanen, and Z. Sun, Adv. Mater. **30**, 1705963 (2018).
18. D. Li, H. Jussila, L. Karvonen, G. Ye, H. Lipsanen, X. Chen, and Z. Sun, Sci. Rep. **5**, 15899 (2015).
19. D. Li, A. E. Castillo, H. Jussila, G. Ye, Z. Ren, J. Bai, X. Chen, H. Lipsanen, Z. Sun, and F. Bonaccorso, Appl. Mater. Today **4**, 17 (2016).
20. A. Autere, C. R. Ryder, A. Saynatjoki, L. Karvonen, B. Amirsolaimani, R. A. Norwood, N. Peyghambarian, K. Kieu, H. Lipsanen, M. C. Hersam, and Z. Sun, J. Phys. Chem. Lett. **8**, 1343 (2017).
21. Z. Sun, A. Martinez, and F. Wang, Nat. Photonics **10**, 227 (2016).
22. E. Polat and C. Kocabas, Nano Lett. **13**, 5851 (2013).
23. I. Baylam, M. N. Cizmeciyan, S. Ozharar, E. O. Polat, C. Kocabas, and A. Sennaroglu, Opt. Lett. **39**, 5180 (2014).
24. I. Baylam, O. Balci, N. Kakenov, C. Kocabas, and A. Sennaroglu, Opt. Lett. **41**, 910 (2016).
25. E. J. Lee, S. Y. Choi, H. Jeong, N. H. Park, W. Yim, M. H. Kim, J. K. Park, S. Son, S. Bae, S. J. Kim, K. Lee, Y. H. Ahn, K. J. Ahn, B. H. Hong, J. Y. Park, F. Rotermund, and D. Yeom, Nat. Commun. **6**, 6851 (2015).
26. J. Bogusławski, Y. Wang, H. Xue, X. Yang, D. Mao, X. Gan, J. Zhao, Q. Dai, G. Soboń, J. Sotor, and Z. Sun, Adv. Funct. Mater. 1801539 (2018).
27. W. Chen, Q. Q. Sun, M. Xu, S. J. Ding, D. W. Zhang, and L. K. Wang, J. Phys. Chem. C **111**, 6495 (2007).